Fast ground-state-to-ground-state separation of small ion crystals

Tyler H. Guglielmo [1,*] Dietrich Leibfried [2] Stephen B. Libby [1] and Daniel H. Slichter [2]
[1]*Lawrence Livermore National Laboratory, Livermore, California 94550, United States of America*
[2]*National Institute of Standards and Technology, Boulder, Colorado 80305, United States of America*

(Received 16 July 2024; accepted 23 September 2024; published 10 October 2024)

Rapid separation of linear crystals of trapped ions into different subsets is critical for realizing trapped ion quantum computing architectures where ions are rearranged in trap arrays to achieve all-to-all connectivity between qubits. We introduce a general theoretical framework that can be used to describe the separation of same-species and mixed-species crystals into smaller subsets. The framework relies on an efficient description of the evolution of Gaussian motional states under quadratic Hamiltonians that only requires a special solution of the classical equations of motion of the ions to describe their quantum evolution under the influence of a time-dependent applied potential and the ions' mutual Coulomb repulsion. We provide time-dependent applied potentials suitable for separation of a mixed-species three-ion crystal on timescales similar to that of free expansion driven by Coulomb repulsion, with all modes along the crystal axis starting and ending close to their ground states. Three separately confined mixed-species ions can be combined into a crystal held in a single well without energy gain by time-reversal of this separation process.

DOI: 10.1103/PhysRevA.110.042610

I. INTRODUCTION

As trapped ion quantum information processors continue to evolve and scale up, efficient all-to-all connectivity becomes increasingly valuable. The quantum charge-coupled device architecture (QCCD) [1] laid out a path for scaling ion trap computers beyond single chains to universal quantum information processors with all-to-all connectivity [1,2]. In recent cutting-edge experimental implementations of the QCCD architecture, the separation, transport, recombination, and recooling of ions consumes 98% or more of the runtime of representative algorithms [3,4]. Separation, transport, and recombination can be classified by whether they occur on timescales lasting many periods of the ion motional modes (adiabatic) or on timescales on the order of the motional period (faster-than-adiabatic or diabatic). Faster-than-adiabatic ion transport with motional modes starting and ending near the ground state has been demonstrated experimentally for crystals of one or two ions of the same species [5–9]. However, separation of multi-ion, multispecies crystals into two subsets with motional modes starting and ending in the ground state (ground-state-to-ground-state separation, or GGS) has only been demonstrated in the adiabatic regime, which is inherently slow [3–5,10–15]. Theoretical work exploring fast GGS has so far been limited to single species or single-ion crystals [16–24]. Furthermore, to achieve many key metrics required of efficient quantum computers, one must be able to achieve efficient GGS. For example, high gate fidelities and short recooling times are difficult or impossible without GGS. Hence, GGS is necessary for essentially all ion connectivity reconfigurations in the QCCD architecture. As such, finding and implementing faster-than-adiabatic GGS protocols is crucial for removing a major speed limitation in current ion trap quantum information processors.

A method for fast GGS was introduced in Ref. [25], wherein two same-species ions initially in a single potential well of a linear rf ion trap were allowed to fly apart through their mutual Coulomb repulsion by rapid removal of the applied confining potential, and then were retrapped in diabatically applied separate potential wells. GGS was achieved in this scenario through special initial-state preparation of the center-of-mass (COM) and stretch normal modes along the crystal axis (axial modes). In particular, the states were squeezed prior to the release of the ions in the initial trap. Since the ion motional states evolve under approximately quadratic Hamiltonians during separation, the unitary time evolution of each mode, from release to recapture, can be represented by a combination of one squeeze operator and one rotation operator, i.e., the Euler decomposition of $SU(1,1) \cong SP(2,\mathbb{R})$ [26–36]. This decomposition allows one to prepare each mode in advance of separation with a squeezing operation that will be exactly undone by the effects of separation, thus enabling capture of the ions in their axial motional ground states after diabatic separation. Although we do not use any of the properties of the groups mentioned above or below explicitly, we mention them by name for expert readers. The key takeaway is that the time evolution operator of our system can be decomposed into a combination of operators, each of which are elements of the symplectic group of n modes, $SP(2n,\mathbb{R})$. The entire protocol is performed in the ion's comoving frame, and any displacements due to residual Coulomb repulsion are negligible at the widely separated final ion positions.

*Contact author: guglielmo2@llnl.gov

Our work extends Ref. [25] to the case of more general linear ion crystal configurations that may contain more than two ions and more than one species. This is accomplished through a combination of squeezing and beam-splitting, i.e., the Bloch-Messiah [29] decomposition of SP(4, $\mathbb{R}$) [30,37–39]. The three-ion crystal we investigate has two modes that remain coupled during time evolution and thus become entangled. The introduction of beam-splitting to the state preparation process is necessary to disentangle the states; single-mode squeezing alone cannot undo the mode-mode entanglement. In addition, rather than presqueezing the axial modes of an ion crystal before separation, we identify suitable time-dependent applied potentials that continuously transform all modes during separation such that they end up close to their ground states in their final potential wells. This "on the fly" transformation should result in further reduction of GGS durations and manifests a method for rapid squeezing that is different from squeezing protocols previously implemented for ion motional modes [40–43]. We present a practically important example, the GGS of a same-species or mixed-species data-helper-data (DHD) three-ion crystal into three separate wells, and we lay out the principles for GGS of larger same- or mixed-species crystals with additional axial modes. The method is general to any choice of data and helper qubit ions, but we specialize to the case of $Be^+-Mg^+-Be^+$ (BMB) for concreteness when discussing a practically relevant example.

In Sec. II we introduce a formalism that is convenient for analyzing Gaussian states and their evolution under quadratic Hamiltonians and will be used throughout the paper. Section III applies this formalism to characterize the squeezing and beam-splitting operations acting on the axial normal modes of a DHD crystal during a swift ramp down of the external potential to zero as well as an equally swift ramp-up of three separate "catching wells"—arresting the three separated ions in analogy to the protocol discussed in Ref. [25]. We then outline the approach for even larger crystals in Sec. III D. Previously, it had been assumed that all state preparation occurred by an unspecified mechanism *prior* to separation [25] or that the modes are returned to their ground states *after* separation is complete. In Sec. IV we overcome this limitation by showing how the states of all three modes in a DHD crystal can be transformed through modulation of the trapping potential while the ions separate to allow for GGS in a three-ion crystal without prior or posterior operations. We find that realistically feasible potential modulation is sufficient to end near the ground states of all three modes and that the protocol is robust against realistic levels of imperfection of the modulation. Concluding remarks in Sec. V summarize the topics introduced in this paper, compare this work to other proposals, and discuss opportunities for future work.

II. THEORETICAL FORMALISM

Before getting into the specifics of any particular ion chain or transport protocol, we will review a theoretical formalism that describes the quantum dynamics of systems undergoing time evolution through quadratic Hamiltonians. The formalism itself is general, however we will only apply it to Gaussian states. More details can be found in [37,44–46].

A. Evolution under quadratic Hamiltonians

We denote the generalized time-independent momentum and position operators of N particles in one dimension as

$$\xi = (p_1, \ldots, p_N, x_1, \ldots, x_N)^T. \tag{1}$$

In our context, these are the momentum and position operators for normal modes of coupled ion motion of N ions along the axis of a linear crystal. Components ξ_a and ξ_b satisfy the following commutation relations:

$$[\xi_a, \xi_b] = i\hbar C_{ab}, \tag{2}$$

$$\boldsymbol{C} = \begin{pmatrix} \mathbf{0} & -\mathbb{I} \\ \mathbb{I} & \mathbf{0} \end{pmatrix}, \tag{3}$$

with $\mathbb{I}$ the N-dimensional identity matrix.

We further assume that the system evolves under a time-dependent purely quadratic Hamiltonian that can be written as

$$H(t) = \tfrac{1}{2}\xi^T \boldsymbol{h}(t)\xi, \tag{4}$$

where $\boldsymbol{h}(t)$ is a Hermitian matrix with dimension $2N \times 2N$. Generalization to include sub-quadratic terms is straightforward and not important for this work. We can now write down how ξ evolves in the Heisenberg picture. Going forward, $\tilde{\xi} = (\tilde{p}_1, \ldots, \tilde{p}_N, \tilde{x}_1, \ldots, \tilde{x}_N)^T$ will represent time-dependent Heisenberg picture operators. Formally, we can write the time evolution as the time-ordered exponential

$$U(t) = \mathcal{T} \exp\left(-\frac{i}{\hbar}\int_0^t H(t')dt'\right), \tag{5}$$

$$\dot{\tilde{\xi}}_a(t) = \frac{i}{\hbar}U^\dagger[H(t), \xi_a]U. \tag{6}$$

Hence,

$$\dot{\tilde{\xi}}(t) = \boldsymbol{C} \cdot \boldsymbol{h}(t)\tilde{\xi}(t), \tag{7}$$

which is equivalent to the classical equations of motion for the momentum and position coordinates, $\Xi = (P_1, \ldots, X_1, \ldots)$. This equation can be rewritten by defining the $2N \times 2N$ transfer matrix $\boldsymbol{M}(t)$,

$$\tilde{\xi}(t) = \boldsymbol{M}(t)\tilde{\xi}_0, \tag{8}$$

which takes $\tilde{\xi}(t=0) = \tilde{\xi}_0$ to some later time t. Inserting into (7) yields

$$\dot{\boldsymbol{M}}(t) = \boldsymbol{C} \cdot \boldsymbol{h}(t) \cdot \boldsymbol{M}(t). \tag{9}$$

With a solution to (9) in hand, the dynamics of $\tilde{\xi}(t)$ are fully determined. From those dynamics, the first and second moments of $\tilde{\xi}$ are also determined. When restricted to Gaussian states, the covariance matrix of $\tilde{\xi}$, $\boldsymbol{V}$, completely determines the state and its elements, and it is given by

$$V_{ij} = \tfrac{1}{2}\langle\{\Delta\tilde{\xi}_i,\ \Delta\tilde{\xi}_j\}\rangle, \tag{10}$$

where $\Delta\tilde{\xi}_i = \tilde{\xi}_i - \langle\tilde{\xi}_i\rangle$, and $\{\cdot,\cdot\}$ is the anticommutator [37]. The covariance matrix then evolves as [37,44,45]

$$\boldsymbol{V}(t) = \boldsymbol{M}(t) \cdot \boldsymbol{V}_0 \cdot \boldsymbol{M}^T(t). \tag{11}$$

Another important factor to consider is that $\boldsymbol{M} \cdot \boldsymbol{C} \cdot \boldsymbol{M}^T = \boldsymbol{C}$, which implies $\boldsymbol{M}$ is symplectic, and parametrizes Sp($2N$, $\mathbb{R}$),

the group under which dynamical time evolution occurs [30,38,39,44,45,47].

The matrix $\boldsymbol{M}(t)$ can be Bloch-Messiah decomposed into a combination of multimode interferometers $\boldsymbol{B}(\boldsymbol{\theta}_k)$ and single-mode squeezers $\boldsymbol{S}(r_k, \phi_k)$ as [29,37,44,48]

$$\boldsymbol{M}(t) = \boldsymbol{B}(\boldsymbol{\theta}_2) \cdot \left[\bigoplus_{k=1}^{N} \boldsymbol{S}(r_k, \phi_k)\right] \cdot \boldsymbol{B}(\boldsymbol{\theta}_1), \tag{12}$$

where $\boldsymbol{\theta}_k$, ϕ_k, and r_k will in general be time-dependent, and $\boldsymbol{\theta}_k$ are Hermitian matrices composed of rotation angles and mixing angles that determine couplings between different modes. The interferometers and squeezers have the functional form

$$\boldsymbol{B}(\boldsymbol{\theta}) = e^{i\boldsymbol{a}^\dagger \cdot \boldsymbol{\theta} \cdot \boldsymbol{a}}, \tag{13}$$

$$\boldsymbol{S}(r_k, \phi_k) = \exp\left[\frac{r_k}{2}\left((a_k^\dagger)^2 e^{i\phi_k} - a_k^2 e^{-i\phi_k}\right)\right], \tag{14}$$

where $\boldsymbol{a} = (a_1, \ldots, a_N)$, and the ladder operators of mode k are denoted as a_k and $a_k^\dagger$. For two modes, a two-port interferometer is equivalent to the application of a beam-splitter and a rotation [49,50]

$$\boldsymbol{B}(\boldsymbol{\theta}) = \boldsymbol{B}_{BS}(\theta_{BS}, \phi_{BS}) \cdot [\boldsymbol{R}_1(\theta_1) \oplus \boldsymbol{R}_2(\theta_2)] \tag{15}$$

$$\equiv \boldsymbol{B}_{BS}(\theta_{BS}, \phi_{BS}) \cdot \boldsymbol{R}_{12}(\theta_1, \theta_2) \tag{16}$$

with

$$\boldsymbol{B}_{BS}(\theta_{BS}, \phi_{BS}) = \exp[\theta_{BS}(a_a^\dagger a_b e^{i\phi_{BS}} - a_a a_b^\dagger e^{-i\phi_{BS}})] \tag{17}$$

and

$$\boldsymbol{R}_k(\theta_k) = \exp[-i\theta_k a_k^\dagger a_k], \tag{18}$$

$$\boldsymbol{R}_{lm}(\theta_l, \theta_m) = \boldsymbol{R}_l(\theta_l) \oplus \boldsymbol{R}_m(\theta_m). \tag{19}$$

A detailed explanation on how this decomposition in (12) is performed can be found in [51].

Crucially, this tells us that the dynamics of any time-dependent quadratic Hamiltonian can be decomposed as a combination of single-mode squeezers and beam-splitting operations. This enables efficient computation of suitable further squeezing and beam-splitting operations, either before or after $H(t)$ acts, that compensate for the effects of $\boldsymbol{M}(t)$ on the initial ground states and will result in final ground states, generally in a basis that can be different from the initial phase-space basis. Formally, if $\boldsymbol{Q}$ is the orthogonal matrix that transforms the initial operators $\tilde{\xi}_0$ that diagonalize $H(0)$ into a set of operators $\tilde{\xi}_t$ that diagonalize $H(t)$, then for GGS

$$\boldsymbol{T} \cdot \boldsymbol{M}(t) = \boldsymbol{M}(t) \cdot \boldsymbol{T}' = \boldsymbol{Q}, \tag{20}$$

where $\boldsymbol{T}$ ($\boldsymbol{T}'$) are suitable compensation operations composed of single-mode squeezers, multiport interferometers, and rotations applied after (before) $H(t)$ has acted. Special cases of this general principle for a single normal mode of ion motion, and for two decoupled normal modes, were explored in [25]. We will discuss the more general separation of a DHD crystal in more detail in Sec. III. Alternatively, a specific $\boldsymbol{h}(t)$ can be identified such that no initial or final operation is necessary for GGS,

$$\boldsymbol{M}(t) = \boldsymbol{Q}, \tag{21}$$

which removes the necessity to compensate for the effects of $H(t)$ and potentially reduces the total duration of all operations necessary for GGS. This approach to separation of a DHD crystal is discussed in Sec. IV.

In both cases, since $\boldsymbol{M}(t)$ represents a unitary time evolution of the system, the equations of motion are invariant under time reversal. As long as this is the case, the operators $\boldsymbol{M}(t)$, $\boldsymbol{T}$, and $\boldsymbol{T}'$ can be inverted to run the process in reverse. This implies that a good solution for ion separation also yields a good solution for the time-reversed process, namely ion recombination.

B. Occupation numbers from the covariance matrix

Given a quadratic Hamiltonian, we would like to track various mode occupation numbers over time. For example, if the curvature of a potential well is changing in time, we may be interested in tracking the occupation numbers of the normal modes of ions confined in the well. In the previous section, we explained how the covariance matrix of a Gaussian state evolves in time under a quadratic Hamiltonian. The occupation number for a mode k with frequency ω_k that remains uncoupled from all other modes at all times has expectation value

$$\langle n_k \rangle = \frac{\langle H_k(t) \rangle}{\hbar\omega_k} - \frac{1}{2}, \tag{22}$$

where $H_k(t)$ is the decoupled subsystem's Hamiltonian. The Hamiltonian's expectation value can be computed from the isolated block in the covariance matrix $\boldsymbol{V}$ of the whole system corresponding to mode k as

$$\langle H_k(t) \rangle = \frac{1}{2m} V_{11}(t) + \frac{1}{2} m\omega_k^2 V_{22}(t), \tag{23}$$

where the matrix subscripts indicate the row and column of the covariance matrix element. In general, when modes are coupled they do not have a well-defined occupation number. However, if a mode is decoupled at any time (for example at late times in a separation protocol, when the ions are far apart from each other), we can extend the definition at that time to all times to define a quantity of interest. A natural choice of modes are the final modes of a separated crystal. After separating an ion crystal into individual potential wells, the final modes will be completely decoupled as the Coulomb repulsion between ions will be negligible, and each ion can be considered individually. Throughout this paper, we will make the choice to compute occupation number with respect to the final modes of a DHD crystal. For example, if two modes, j and k, are coupled initially, but decoupled at late times with potential strengths $\omega_{j,k}$, we can define the following quantities derived from their covariance matrix $\boldsymbol{V}^{jk}$ at all times:

$$\langle n_j \rangle = \frac{\frac{1}{2m_j} V_{11}^{jk}(t) + \frac{1}{2} m_j \omega_j^2 V_{33}^{jk}(t)}{\hbar\omega_j} - \frac{1}{2}, \tag{24}$$

$$\langle n_k \rangle = \frac{\frac{1}{2m_k} V_{22}^{jk}(t) + \frac{1}{2} m_k \omega_k^2 V_{44}^{jk}(t)}{\hbar\omega_k} - \frac{1}{2}. \tag{25}$$

This can be generalized to M coupled modes that are uncoupled at some time, but the dimension of the block of correlations in the covariance matrix of the full system that needs to be considered increases to $2M \times 2M$.

III. TWO-SPECIES THREE-ION (DHD) CRYSTAL

We will now show how GGS can be performed in a linear DHD crystal, which we treat in one spatial dimension x along the crystal axis. The ion species under consideration are unimportant for this work, however for concreteness when performing numerical calculations we choose the mass m_D of D equal to that of $^9Be^+$ and m_H of H equal to that of $^{25}Mg^+$.

In the separation considered here, we assume that a linear DHD crystal is aligned along the weakest axis of the trapping potential, and its axial normal modes are cooled to near their ground states, with the expectation values of the axial ion positions equal to the classical equilibrium positions of the ions denoted by c_{D1}, c_{D2}, and c_H, which will become time-dependent during the separation protocol. The H species ion is held in between the two D species ions. The applied harmonic confining potential at the ion positions is defined in terms of a local spring constant $k_H(t)$ at the H ion and $k_D(t)$ at the D ions. When this potential is removed, the two D ions are pushed apart by the three ions' mutual Coulomb repulsion, while the H ion ideally remains stationary at the origin at all times. After some amount of time, the D ions have reached a sufficient distance such that approximately harmonic potentials local to each ion can be turned back on with negligible interference between the three wells, thus trapping each ion individually. When neglecting the residual Coulomb repulsion at the final ion distances, the separate potential well minimum locations w_{D1} and w_{D2} coincide with the classical positions c_{D1} and c_{D2} of the D ions, symmetrically displaced from the origin where the H ion remained during the separation.

This can be described by the classical Hamiltonian

$$\begin{aligned}\mathcal{H}(t) = &\frac{p_{D1}^2 + p_{D2}^2}{2m_D} + \frac{p_H^2}{2m_H} + \frac{1}{2}k_D(t)[(c_{D1} - w_{D1})^2 \\ &+ (c_{D2} - w_{D2})^2] + \frac{1}{2}k_H(t)c_H^2 + \frac{k_e q^2}{c_H - c_{D1}} \\ &+ \frac{k_e q^2}{c_{D2} - c_{D1}} + \frac{k_e q^2}{c_{D2} - c_H},\end{aligned} \tag{26}$$

where p_{D1}, p_{D2}, and p_H are the momenta of the three ions, q is the elementary charge, and $k_e = 1/(4\pi\epsilon_0)$ is the electrostatic constant derived from the vacuum permittivity ϵ_0. We note that the c and w values are time-dependent, although we have not written this explicitly in (26). The DHD crystal is arranged such that $c_{D1} < c_H = 0 < c_{D2}$ so all denominators in the Coulomb interaction terms are positive throughout the separation. We make the approximation that the classical position of the H ion remains fixed, $c_H(t) = 0$, and we do not consider perturbations of its position at this point. This approximation also implies $c_{D2}(t) = -c_{D1}(t) \equiv c(t)$ and $w_2(t) = -w_1(t) = w(t)$, with $w_H(t) = 0$.

To model the small oscillations of the ions around their classical motion quantum mechanically, we can transform into a frame of reference moving along the classical trajectory $c_{D1}(t)$, $c_{D2}(t)$, and $c_H(t)$ for each ion [determined by solving (26)] by applying appropriate displacement operators. We refer the reader to the supplemental material in [25] for a complete discussion on this transformation. The procedure follows by writing the quantum version of (26) and applying displacement operators to the Hamiltonian so that the position and momentum transform as

$$p_j \to p_j + m_j\dot{c}_j(t), \quad x_j \to x_j + c_j(t). \tag{27}$$

We can then introduce mass weighted quantum-mechanical operators

$$p_j \to \sqrt{m_j}p_j, \quad x_j \to \frac{x_j}{\sqrt{m_j}} \tag{28}$$

to describe small displacements relative to the classical frame of reference and accommodate ions of different mass. This rescaling has the effect of changing the units of the new x and p operators to $\sqrt{\text{kg}}\,\text{m}$ and $\sqrt{\text{kg}}\,\text{m/s}$, respectively. The unit of the Hamiltonian remains J. Under the assumption that the real space (non-mass-weighted) displacements are much smaller than the relative distances between ions, we can also expand the Coulomb term to quadratic order. We have not yet detailed the specific procedure for separation that we will employ, however we can justify this approximation for the separation procedure employed later on because the largest value of the cubic correction (when the ions are closest together) is still a factor of ~60 smaller than the quadratic term, and it becomes negligible after any substantial separation. Furthermore, as we are making the approximation that $c_H(t) = 0$, and that all applied potentials remain symmetric, cubic terms will not contribute to the first-order energy correction in perturbation theory as the expectation value of a cubic term with a squeezed state is 0. The quartic term is a factor ~6000 smaller than the quadratic term at closest ion approach and it can be neglected safely. Indeed, including cubic and quartic terms into our simulation for results presented later on reproduces nearly indistinguishable results. However, we have only proven this approximation for procedures with nonlinearities of the same size as the protocol we employ later on—any speedups to this protocol will most likely introduce larger nonlinear corrections that must be taken into consideration.

Reinterpreting the displaced classical position and momentum variables in (27) as quantum-mechanical operators, we arrive at a quantum-mechanical Hamiltonian corresponding to three coupled harmonic oscillators:

$$\begin{aligned}H(t) \approx &\frac{1}{2}\left[p_{D1}^2 + p_{D2}^2 + p_H^2\right] + \frac{1}{2}\frac{k_D(t)}{m_D}\left[x_{D1}^2 + x_{D2}^2\right] + \frac{1}{2}\frac{k_H(t)}{m_H}x_H^2 \\ &+ \frac{k_e q^2}{c^3(t)}\left[\frac{x_{D1}^2 + x_{D2}^2}{m_D} + \frac{2x_H^2}{m_H} + \frac{(x_{D2} - x_{D1})^2}{8m_D} - \frac{2x_H(x_{D1} + x_{D2})}{\sqrt{m_D m_H}}\right].\end{aligned} \tag{29}$$

As long as the separating ions are sufficiently closely approximated by (29), the general formalism described in Sec. II can be applied to describe the ensuing dynamics.

We can partially decouple the oscillators by introducing in-phase and out-of-phase coordinates for the D ions,

$$x_{\rm op} = \frac{x_{D2} - x_{D1}}{\sqrt{2}}, \qquad x_{\rm ip} = \frac{x_{D2} + x_{D1}}{\sqrt{2}}, \tag{30}$$

$$p_{\rm op} = \frac{p_{D2} - p_{D1}}{\sqrt{2}}, \qquad p_{\rm ip} = \frac{p_{D2} + p_{D1}}{\sqrt{2}}, \tag{31}$$

along with corresponding time-dependent oscillator frequencies

$$\begin{aligned}\omega_{\rm op}^2(t) &= \frac{k_D(t)}{m_D} + \frac{5k_eq^2}{2m_Dc^3(t)},\\ \omega_{\rm ip}^2(t) &= \frac{k_D(t)}{m_D} + \frac{2k_eq^2}{m_Dc^3(t)},\\ \omega_H^2(t) &= \frac{k_H(t)}{m_H} + \frac{4k_eq^2}{m_Hc^3(t)},\end{aligned} \tag{32}$$

and mode-coupling strength

$$\Omega_{H\rm ip}^2(t) = \frac{4\sqrt{2}\,k_eq^2}{\sqrt{m_Dm_H}\,c^3(t)}. \tag{33}$$

The Hamiltonian can then be written as

$$H(t) = \frac{1}{2}\sum_{k={\rm ip,op},H}\left[p_k^2 + \omega_k^2(t)x_k^2\right] - \Omega_{H\rm ip}^2(t)x_Hx_{\rm ip}, \tag{34}$$

which has the form of the Hamiltonian in (4) with an out-of-phase mode that is decoupled from the other two modes and has no participation of the H ion. The other two modes are coupled initially with a term that is linear in their position operators and therefore acts in analogy to a beam-splitter. Inspection of (32) reveals that the terms proportional to the Coulomb interaction fall off as $1/c^3(t)$ and rapidly become negligible compared to the confinement $k_D(t)$ from the external potential towards the end of separation. This justifies the approximation of three decoupled oscillators at the end of separation with motional frequencies determined entirely by the local curvature of the external potential and the mass of the ions.

Applying a suitable time-dependent basis rotation between the two coupled modes will allow us to write the Hamiltonian in a way that is fully decoupled whenever the oscillator frequencies are not changing in time (in particular, before and after separation). However, the modes can still be coupled at intermediate times. To this end, we can define two new normal modes, a and b, as well as their operators, x_a and x_b that are connected to the H and in-phase modes by the unitary transformation

$$U_\theta = \exp\left[-\frac{i}{\hbar}\theta\left(p_Hx_{\rm ip} - p_{\rm ip}x_H\right)\right], \tag{35}$$

where θ is implicitly defined as

$$\tan 2\theta = \frac{2\Omega_{H\rm ip}^2}{\omega_H^2 - \omega_{\rm ip}^2}. \tag{36}$$

The position operators in the rotated basis are

$$\begin{aligned}x_a &= U_\theta x_{\rm ip}U_\theta^\dagger = x_{\rm ip}\cos\theta + x_H\sin\theta,\\ x_b &= U_\theta x_HU_\theta^\dagger = x_H\cos\theta - x_{\rm ip}\sin\theta.\end{aligned} \tag{37}$$

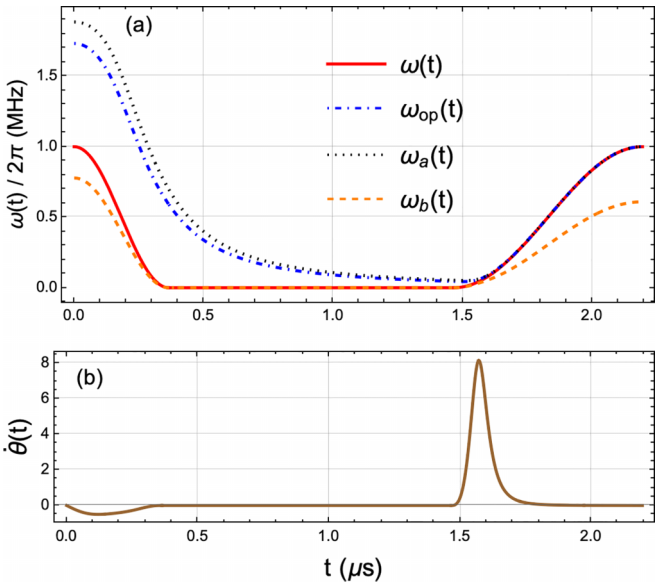

FIG. 1. Plots of the frequencies and $\dot\theta$ over time. (a) Plots of frequencies over time. Here $\omega(t)$ is the frequency that describes the external trapping potential strength and is given in (42), and $\omega_{\rm op}(t)$ describes the full potential experienced by the out-of-phase mode as given by (32). Similarly, $\omega_a(t)$ and $\omega_b(t)$ describe the full potential experienced by the a and b modes as given by (39) and (40). At $t = 0$ the trapping potential is ramped down from the equilibrium strength over 0.365 μs. At $t = 1.465$ μs the potential begins ramping up over 0.73 μs. Note that the final values of $\omega(t)$, $\omega_{\rm op}(t)$, and $\omega_a(t)$ are all the same, while $\omega_b(t)$ is distinct. This is occurs because $\omega_{\rm op}(t)$ and $\omega_a(t)$ approach the mode frequency of the two D ions, while $\omega_b(t)$ approaches that of the H ion. (b) Plot of the coupling $\dot\theta(t)$ over time. This coupling is only active during the potential ramps.

Since θ changes in time, this basis is constantly adjusting as the separation proceeds. In the adjusted basis, the Hamiltonian transforms to

$$\begin{aligned}H_\theta = U_\theta H(t)U_\theta^\dagger + i\dot U_\theta U_\theta^\dagger = \frac{p_{ip}^2 + p_a^2 + p_b^2}{2} + \frac{1}{2}\omega_{\rm ip}^2(t)x_{\rm ip}^2\\ + \frac{1}{2}\omega_a^2(t)x_a^2 + \frac{1}{2}\omega_b^2(t)x_b^2 + \dot\theta(p_bx_a - p_ax_b),\end{aligned} \tag{38}$$

where we have defined the following quantities:

$$\omega_a^2 = \tfrac{1}{2}\left(\omega_{\rm ip}^2 + \omega_H^2 + \Gamma\right), \tag{39}$$

$$\omega_b^2 = \tfrac{1}{2}\left(\omega_{\rm ip}^2 + \omega_H^2 - \Gamma\right), \tag{40}$$

$$\Gamma = \sqrt{4\Omega_{H\rm ip}^4 + \left(\omega_{\rm ip}^2 - \omega_H^2\right)^2}. \tag{41}$$

A full exploration of this type of transformation in two dimensions can be found in [23]. In the chosen frame of reference, all modes are decoupled whenever $\dot\theta = 0$. Additionally, the position of one oscillator is coupled to the momentum of the other in this frame, which can be seen from the last term in (38). This coupling between the a and b modes will generate entanglement during the time evolution.

A. Classical dynamics

For separation of the DHD crystal in a physical system, the applied confining potential cannot be turned on and off instantaneously due to experimental constraints. For concreteness and ease of calculation in the following examples, we use sinusoidal ramping of the potential in time, but other ramp shapes could also be used. We ramp the external axial potential to zero starting at $t = 0$ over a duration τ, followed by expansion of the ion crystal for τ_0 and another sinusoidal ramp to retrap the ions in separate wells with duration τ, in analogy to the separation considered in [25]. Writing out the time dependence explicitly and denoting $\omega_0 = \sqrt{k_D(0)/m_D}$,

$$\omega(t) = \begin{cases} \omega_0, & t \leqslant 0, \\ \frac{\omega_0}{2}\left[1 + \cos\left(\frac{\pi}{\tau}t\right)\right], & 0 < t \leqslant \tau, \\ 0, & \tau < t \leqslant \tau + \tau_0, \\ \frac{\omega_0}{2}\left[1 - \cos\left(\frac{\pi(t-\tau-\tau_0)}{\tau}\right)\right], & \tau + \tau_0 < t \leqslant 2\tau + \tau_0, \\ \omega_0, & t > 2\tau + \tau_0, \end{cases} \tag{42}$$

where $\omega^2(t) = k_D(t)/m_D = k_H(t)/m_D$. The time dependence of (32), (39), (40), and (42) is shown in Fig. 1.

It is necessary to ensure that the classical motion of all three ions leaves them at rest at the end of the separation. While the initial potential confines the ions, $t \in (-\infty, \tau]$, the potential minimum is located at the origin, $w_i(t < \tau) = 0$. However, during the retrapping period, we will allow the potential to move and apply forces to the D ions to slow them down. To this end, the potential minima near the D ions will follow

$$w_1(t) = c_{D1}(t) - \eta \dot{c}_{D1}(t) \tag{43}$$

and analogously for w_2 with c_{D2}. This introduces decelerating forces proportional to the ion velocities in the classical dynamics, which slow the ions as they are recaptured and cease once the ions are at rest.

B. State preparation

To achieve GGS, we can cool the motional modes close to their ground states and precompensate for the quantum-mechanical effects of separation during $t < 0$, then separate the crystal starting at $t = 0$ to end in the ground states of all three final modes at t_f. We can separate (38) into the time evolution of two states. The in-phase mode is completely decoupled from the rest of the Hamiltonian and can be evolved independently. The a and b modes are decoupled at $t = 0$, couple during separation (implying that their motion is entangled), and decouple at $t = t_f = 2\tau + \tau_0$. They must be evolved together, and any state preparation must not only involve single-mode squeezing but also two-mode entangling operations such as beam-splitting. The time evolution during separation can be further decomposed into suitable squeezing operations $\boldsymbol{S}(r_k, \phi_k)$ on the kth initial normal mode with ($k = \{\mathrm{op}, a, b\}$), rotation operations $\boldsymbol{R}(\theta_k)$ on the kth initial normal mode, and a beam-splitting operation $\boldsymbol{B}_{BS}(\theta_{BS}, \phi_{BS})$ between modes a and b as defined in (12)–(18). In the phase-space coordinates introduced in Sec. II, these operations take the form

$$\begin{pmatrix} p_k \\ x_k \end{pmatrix}_S = \boldsymbol{S}(r_k, \phi_k)\begin{pmatrix} p_k \\ x_k \end{pmatrix}_0 = \begin{pmatrix} \cosh(r_k) - \sinh(r_k)\cos(\phi_k) & \omega_k \sinh(r_k)\sin(\phi_k) \\ \frac{1}{\omega_k}\sinh(r_k)\sin(\phi_k) & \cosh(r_k) + \sinh(r_k)\cos(\phi_k) \end{pmatrix}\begin{pmatrix} p_k \\ x_k \end{pmatrix}_0, \tag{44}$$

$$\begin{pmatrix} p_k \\ x_k \end{pmatrix}_R = \boldsymbol{R}(\theta_k)\begin{pmatrix} p_k \\ x_k \end{pmatrix}_0 = \begin{pmatrix} \cos\theta_k & -\omega_k \sin\theta_k \\ \frac{1}{\omega_k}\sin\theta_k & \cos\theta_k \end{pmatrix}\begin{pmatrix} p_k \\ x_k \end{pmatrix}_0, \tag{45}$$

$$\begin{pmatrix} p_a \\ p_b \\ x_a \\ x_b \end{pmatrix}_{BS} = \begin{pmatrix} \cos\theta_{BS} & \sqrt{\frac{\omega_a}{\omega_b}}\cos(\phi_{BS})\sin(\theta_{BS}) & 0 & \sqrt{\omega_a\omega_b}\sin(\phi_{BS})\sin(\theta_{BS}) \\ -\sqrt{\frac{\omega_b}{\omega_a}}\cos(\phi_{BS})\sin(\theta_{BS}) & \cos\theta_{BS} & \sqrt{\omega_a\omega_b}\sin(\phi_{BS})\sin(\theta_{BS}) & 0 \\ 0 & \frac{-1}{\sqrt{\omega_a\omega_b}}\sin(\phi_{BS})\sin(\theta_{BS}) & \cos\theta_{BS} & \sqrt{\frac{\omega_b}{\omega_a}}\cos(\phi_{BS})\sin(\theta_{BS}) \\ \frac{-1}{\sqrt{\omega_a\omega_b}}\sin(\phi_{BS})\sin(\theta_{BS}) & 0 & -\sqrt{\frac{\omega_a}{\omega_b}}\cos(\phi_{BS})\sin(\theta_{BS}) & \cos\theta_{BS} \end{pmatrix}\begin{pmatrix} p_a \\ p_b \\ x_a \\ x_b \end{pmatrix}_0, \tag{46}$$

where $\omega_k = \omega_k(0)$ and $\omega_{a,b} = \omega_{a,b}(0)$. Writing the operators in this form requires application of the Baker-Campbell-Hausdorff theorem, and it is covered in detail in [46]. The arguments for these operations are determined by the quantum dynamics of the system during separation. In the frame moving with the classical ion positions, these are governed by (38), which we will consider in detail in the next section. To reasonably compensate for the beam-splitting dynamics and squeezing during separation, all three ions need to be in close proximity with substantial Coulomb coupling and resolvable differences in the mode frequencies. For this reason, we will only consider compensation before or during separation here, as opposed to later instances when there is no mode coupling due to spatial separation.

C. Time evolution and occupation numbers

1. Out-of-phase mode

To map an arbitrary state in the initial well at frequency $\omega_{\mathrm{op}}(0) = \sqrt{3}\omega_0$ to its equivalent state in the final well at

frequency $\omega_{\rm op}(t_f) = \omega_0$, the net effect of all operations must be equal to the scaling operator

$$\boldsymbol{Q}_{\rm op} = \begin{pmatrix} \sqrt{\frac{\omega_{\rm op}(t_f)}{\omega_{\rm op}(0)}} & 0 \\ 0 & \sqrt{\frac{\omega_{\rm op}(0)}{\omega_{\rm op}(t_f)}} \end{pmatrix}, \tag{47}$$

which can also be thought of as undoing the effect of the squeezing incurred by the out-of-phase mode due to an instantaneous change in its frequency from $\omega_{\rm op}(0)$ to $\omega_{\rm op}(t_f)$.

In terms of the covariance, the out-of-phase mode's initial ground state at the initial oscillator frequency, $\sqrt{3}\omega_0$, is described by

$$\boldsymbol{V}_{\rm op}(0) \equiv \boldsymbol{V}_{\rm op}^{(i)} = \begin{pmatrix} \frac{\sqrt{3}\hbar\omega_0}{2} & 0 \\ 0 & \frac{\hbar}{2\sqrt{3}\omega_0} \end{pmatrix}, \tag{48}$$

while the covariance matrix of the out-of-phase mode's final state after successful GGS is given by

$$\boldsymbol{V}_{\rm op}(t_f) \equiv \boldsymbol{V}_{\rm op}^{(f)} = \begin{pmatrix} \frac{\hbar\omega_0}{2} & 0 \\ 0 & \frac{\hbar}{2\omega_0} \end{pmatrix}, \tag{49}$$

and $\boldsymbol{Q}_{\rm op} \cdot \boldsymbol{V}_{\rm op}^{(i)} \cdot \boldsymbol{Q}_{\rm op}^T = \boldsymbol{V}_{\rm op}^{(f)}$ as expected.

The effect of separation on the out-of-phase mode can be calculated from $\boldsymbol{h}(t)$ in (4),

$$\boldsymbol{h}_{\rm op}(t) = \begin{pmatrix} 1 & 0 \\ 0 & \omega_{\rm op}^2(t) \end{pmatrix}, \tag{50}$$

which can be inserted into (9) to solve for $\boldsymbol{M}_{\rm op}(t)$ numerically,

$$\begin{aligned} \dot{\boldsymbol{M}}_{\rm op}(t) &= -\boldsymbol{C}_{\rm op} \cdot \boldsymbol{h}_{\rm op}(t) \cdot \boldsymbol{M}_{\rm op}(t), \\ \boldsymbol{M}_{\rm op}(0) &= \boldsymbol{I}, \end{aligned} \tag{51}$$

to yield $\boldsymbol{M}_{\rm op}(t_f) \equiv \boldsymbol{M}_{\rm op}^{(f)}$. The Bloch-Messiah theorem states that $\boldsymbol{M}_{\rm op}^{(f)}$ can be decomposed into squeezing operations and rotations of the form given in (44) and (45), each with unit determinant. Therefore, the inverse is

$$\left(\boldsymbol{M}_{\rm op}^{(f)}\right)^{-1} = \begin{pmatrix} m_{22} & -m_{12} \\ -m_{21} & m_{11} \end{pmatrix}, \tag{52}$$

where m_{jk} are the matrix elements of $\boldsymbol{M}_{\rm op}^{(f)}$. The covariance $\boldsymbol{V}_{\rm op}^{(p)}$ (superscript p denoting precompensated) at $t = 0$, after precompensation but before separation, is

$$\boldsymbol{V}_{\rm op}^{(p)} \equiv \left(\boldsymbol{M}_{\rm op}^{(f)}\right)^{-1} \cdot \boldsymbol{V}_f \cdot \left[\left(\boldsymbol{M}_{\rm op}^{(f)}\right)^{-1}\right]^T. \tag{53}$$

The general form of a precompensation operation is

$$\begin{aligned} \boldsymbol{M}_{\rm op}^{(p)} &= \boldsymbol{R}_p(\theta_2) \cdot \boldsymbol{S}_p(r, \phi) \cdot \boldsymbol{R}_p(\theta_1) \\ &= \boldsymbol{R}_p(\theta_2) \cdot \boldsymbol{S}_p(r, \phi) \cdot \boldsymbol{R}_p(-\theta_2) \cdot \boldsymbol{R}_p(\theta_2) \cdot \boldsymbol{R}_p(\theta_1) \\ &= \boldsymbol{S}_p(r_p, \phi_p) \cdot \boldsymbol{R}_p(\theta_p), \end{aligned} \tag{54}$$

where $\theta_p = \theta_1 + \theta_2$, $r_p = r$, and $\phi_p = \phi + 2\theta_2$ are parameters that are not yet determined. Since $\boldsymbol{V}_0$ is the covariance of a Gaussian state, $\boldsymbol{R}_p(\theta) \cdot \boldsymbol{V}_p(0) \cdot \boldsymbol{R}_p^T(\theta) = \boldsymbol{V}_{\rm op}(0)$ for any θ. After precompensation, the covariance matrix of the initial state takes the form

$$\boldsymbol{V}_{\rm op}^{(p)} = \boldsymbol{S}_p(r_p, \phi_p) \cdot \boldsymbol{V}_{\rm op}^{(i)} \cdot \boldsymbol{S}_p^T(r_p, \phi_p). \tag{55}$$

By inserting (44) into (55) and comparing to (53) element by element, we find

$$\cosh(2r_p) = \frac{\left(\frac{m_{12}}{\omega_0}\right)^2 + 3m_{11}^2 + \left(m_{22}^2 + 3m_{21}^2\omega_0^2\right)}{2\sqrt{3}}, \tag{56}$$

$$\sin(\phi_p) = -\frac{m_{11}m_{12} + m_{22}m_{21}\omega_0^2}{\omega_0 \sinh 2r_p}. \tag{57}$$

For a concrete example, we assume a BMB crystal with initial axial in-phase frequency $\omega_{\rm ip}/2\pi = 1$ MHz, where $\omega^2(t)$ is ramped down over $\tau = 0.365\,\mu$s. The ions are allowed to fly apart unimpeded for $\tau_0 = 1.1\,\mu$s, and the potentials are ramped back up over $2\tau = 0.73\,\mu$s. The required presqueezing parameters are $r_p \approx 1.597$ and $\phi_p \approx -0.671$. The total duration of separation is similar to the two-ion separation discussed in [25], which is reasonable given that similar Coulomb repulsion forces, ion masses, and final relative distances are used.

The correct parameters for precompensation and the numerical solution for $\boldsymbol{M}_{\rm op}(t)$ allows us to compute the occupation number of the out-of-phase mode as a function of time with respect to the final well frequency ω_0 from $t = 0$ to t_f,

$$\langle n_{\rm op}\rangle_t = \frac{\frac{1}{2}V_{11}^{\rm op}(t) + \frac{1}{2}\omega_0^2 V_{22}^{\rm op}(t)}{\hbar\omega_0} - \frac{1}{2}. \tag{58}$$

Figure 2 shows (a) the position and strength of the potential wells and the classical time evolution of the position of the three ions, and (b) the out-of-phase mode's occupation number over time.

2. The a and b modes

As with the out-of-phase mode, the initial state must be precompensated before separation starts at $t = 0$, but now with a suitable combination of single-mode squeezing operations for a and b individually as well as a two-port interferometer. The initial and final normal mode frequencies in (38) are

$$\begin{aligned} \omega_a(0) &= \frac{\omega_0}{\sqrt{10}}\sqrt{13 + 21\frac{m_D}{m_H} + \sqrt{\frac{512m_D}{m_H} + \left(13 - 21\frac{m_D}{m_H}\right)^2}} \\ &\equiv \alpha_a\omega_0, \\ \omega_a(t_f) &= \omega_0, \\ \omega_b(0) &= \frac{\omega_0}{\sqrt{10}}\sqrt{13 + 21\frac{m_D}{m_H} - \sqrt{\frac{512m_D}{m_H} + \left(13 - 21\frac{m_D}{m_H}\right)^2}} \\ &\equiv \alpha_b\omega_0, \\ \omega_b(t_f) &= \sqrt{\frac{m_D}{m_H}}\omega_0 \equiv \beta_b\omega_0. \end{aligned} \tag{59}$$

When applied to modes in their ground states initially, the interferometer $\boldsymbol{B}(\boldsymbol{\theta}_1)$ in the decomposition (12) of the precompensation operation has no effect. It is sufficient to squeeze the two modes followed by an interferometer,

$$\boldsymbol{M}_{ab}^{(p)} = \boldsymbol{B}_{ab}(\boldsymbol{\theta})[\boldsymbol{S}_a(r_a, \phi_a) \oplus \boldsymbol{S}_b(r_b, \phi_b)]. \tag{60}$$

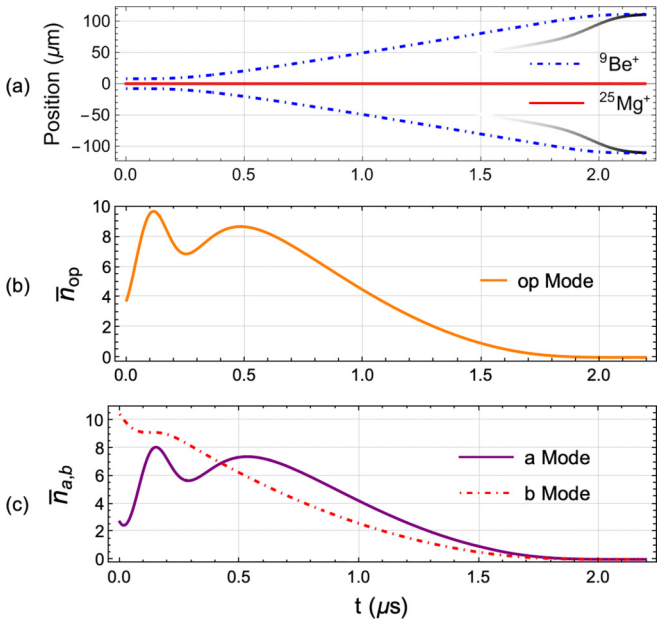

FIG. 2. Numerical solutions for classical ion positions and all three modes' mean occupation number. (a) Classical time evolution of the three-ion BMB crystal. At $t = 0$ the trapping potential is ramped down from the equilibrium strength over 0.365 μs. At $t = 1.465$ μs the potential begins ramping up over 0.73 μs. This amounts to a total separation time of ∼2.2 μs without accounting for state preparation. The grayscale with varying opacity indicates individual trapping potential locations for the B ions as well as strength, with higher opacity indicating stronger confinement. The M ion ideally remains in place with its confining potential strength ramped simultaneously with those for the B but not shown in the figure. (b) Mean occupation number of the out-of-phase mode during time evolution. (c) Mean occupation numbers of the a and b modes during time evolution.

This can be further reduced by making use of (15) and the insertion of rotation operators, remembering that rotations leave the ground state invariant,

$$\begin{aligned} \boldsymbol{M}_{ab}^{(p)} &= \boldsymbol{B}_{BS}(\theta_{BS},\phi_{BS})\cdot\boldsymbol{R}_{ab}(\theta_a,\theta_b)[\boldsymbol{S}_a(r_a,\phi_a)\oplus\boldsymbol{S}_b(r_b,\phi_b)] \\ &\quad\times\boldsymbol{R}_{ab}(-\theta_a,-\theta_b)\cdot\boldsymbol{R}_{ab}(\theta_a,\theta_b) \qquad (61)\\ &= \boldsymbol{B}_{BS}(\theta_{BS},\phi_{BS})[\boldsymbol{S}_a(r_a,\phi_a')\oplus\boldsymbol{S}_b(r_b,\phi_b')]\boldsymbol{R}_{ab}(\theta_a,\theta_b) \qquad (62)\\ &\to \boldsymbol{B}_{BS}(\theta_{BS},\phi_{BS})[\boldsymbol{S}_a(r_a,\phi_a')\oplus\boldsymbol{S}_b(r_b,\phi_b')]. \qquad (63)\end{aligned}$$

The covariance matrix of the initial state is

$$\boldsymbol{V}_{ab}^{(i)} = \begin{pmatrix} \frac{\alpha_a\hbar\omega_0}{2} & 0 & 0 & 0\\ 0 & \frac{\alpha_b\hbar\omega_0}{2} & 0 & 0\\ 0 & 0 & \frac{\hbar}{2\alpha_a\omega_0} & 0\\ 0 & 0 & 0 & \frac{\hbar}{2\alpha_b\omega_0}\end{pmatrix}, \qquad (64)$$

and that of the final state is

$$\boldsymbol{V}_{ab}^{(f)} = \begin{pmatrix} \frac{\hbar\omega_0}{2} & 0 & 0 & 0\\ 0 & \frac{\beta_b\hbar\omega_0}{2} & 0 & 0\\ 0 & 0 & \frac{\hbar}{2\omega_0} & 0\\ 0 & 0 & 0 & \frac{\hbar}{2\beta_b\omega_0}\end{pmatrix}. \qquad (65)$$

For the the a and b modes, $\boldsymbol{h}(t)$ in (4) takes the form

$$h_{ab}(t) = \begin{pmatrix} 1 & 0 & 0 & -\dot\theta(t)\\ 0 & 1 & \dot\theta(t) & 0\\ 0 & \dot\theta(t) & \omega_a^2(t) & 0\\ -\dot\theta(t) & 0 & 0 & \omega_b^2(t)\end{pmatrix}. \qquad (66)$$

The equation of motion for $\boldsymbol{M}_{ab}$ is

$$\dot{\boldsymbol{M}}_{ab}(t) = -\boldsymbol{C}\cdot\boldsymbol{h}_{ab}(t)\cdot\boldsymbol{M}_{ab}(t), \qquad (67)$$

$$\boldsymbol{M}_{ab}(0) = \boldsymbol{I}, \qquad (68)$$

and it can be solved numerically with $\boldsymbol{M}_{ab}(t_f)\equiv\boldsymbol{M}_{ab}^{(f)}$ and inverted to yield

$$\boldsymbol{V}_{ab}^{(p)} \equiv \left(\boldsymbol{M}_{ab}^{(f)}\right)^{-1}\cdot\boldsymbol{V}_{ab}^{(f)}\cdot\left[\left(\boldsymbol{M}_{ab}^{(f)}\right)^{-1}\right]^T, \qquad (69)$$

which can be compared to

$$\boldsymbol{V}_{ab}^{(p)} = \boldsymbol{M}_{ab}^{(p)}\cdot\boldsymbol{V}_{ab}^{(i)}\cdot\left[\boldsymbol{M}_{ab}^{(p)}\right]^T \qquad (70)$$

to find the correct parameters for precompensation numerically.

The squeezing parameters required for GGS on the a and b modes in this BMB crystal are $r_a \approx 1.938$ and $r_b \approx 1.483$, respectively, with phases $\phi_a \approx -1.846$ and $\phi_b \approx -2.902$. The required beam-splitting parameters are $\theta_B \approx 1.714$, and $\phi_B \approx -1.470$. In analogy to the out-of-phase mode, the occupation numbers for both modes can be written as

$$\langle n_a\rangle_t = \frac{\frac{1}{2}V_{11}^{ab}(t)+\frac{1}{2}\omega_0^2V_{33}^{ab}(t)}{\hbar\omega_0}-\frac{1}{2}, \qquad (71)$$

$$\langle n_b\rangle_t = \frac{\frac{1}{2}V_{22}^{ab}(t)+\frac{1}{2}(\beta_b\omega_0)^2V_{44}^{ab}(t)}{\beta_b\hbar\omega_0}-\frac{1}{2}, \qquad (72)$$

and they are shown in Fig. 2(c).

D. Generalization to larger crystals

The generalization of this procedure to larger crystals is not difficult but rather tedious. For example, a crystal such as DHHD will have four modes that decouple into two groups of coupled oscillators. Each group will have its own rotation angle $\theta_{1,2}$ and appear in the same way as the rotation appears in (38). In this way, state preparation can be done on the two groups individually through two groups of single-mode squeezers and beam-splitters.

The generalization to crystals such as D$\cdots$DHD$\cdots$D with N ions, for odd N, is again straightforward, but it requires a slightly more complicated decoupling procedure where we end up with two groups. The first group contains $X = (N+1)/2$ coupled modes described by in-phase modes with participation from the $N-1$ data qubits as well as the helper ion. The second group contains $Y = (N-1)/2$ coupled out-of-phase modes for the $N-1$ data qubits in which

the helper ion does not participate. The state preparation for such a crystal will require X single-mode squeezers and an X-port interferometer on the first mode group as well as Y single-mode squeezers and a Y-port interferometer on the second mode group.

E. Timescales for precompensation

Operations to precompensate the motional modes for GGS require a finite amount of time. Resonant squeezing of a motional mode at frequency ω_k can be accomplished by modulating the potential curvature at $2\omega_k$. To our knowledge, the strongest experimentally demonstrated squeezing rate for a single motional mode is $r = t/(3.2\,\mu\text{s})$ [43]. This rate can potentially be increased, but to keep the effects on spectator modes negligible, the duration of each squeezing operation must be substantially above $1/(2\min[\Delta\omega_{kl}])$, where $\Delta\omega_{kl}$ is the frequency difference between modes k and $l \neq k$. For mode frequencies between $1 \leqslant \omega_k \leqslant 3$ MHz, we estimate a total duration not shorter than approximately 6 μs for all three squeezing operations. A balanced beam-splitter between two axial modes in a three-ion BMB crystal was implemented in 17 μs in [52] by driving a suitable coupling potential at $\Delta\omega_{kl}$. Similar considerations about the spectator mode to those for resonant squeezing apply, and we can estimate a duration no shorter than 2 μs for the beam-splitter operation. Under these assumptions, the total duration of precompensation and separation is on the order of 10 μs, substantially larger than the 2 μs required for the three ions to separate by 80 μm as shown in Fig. 2.

IV. THREE-ION GGS THROUGH ON-THE-FLY COMPENSATION

Since the precompensation removes effects from diabatic changes of the external potential, it seems reasonable that a more elaborate choice of dynamical external potential than just ramping down and back up can separate the ions *and* have all three modes start and end in their ground states in a duration that is on the same timescale as the Coulomb expansion. This external potential can be parametrized through a Fourier series or similar with optimization being performed on its parameters to achieve GGS. This "on-the-fly compensation" will be explored next.

Our starting point is the partially decoupled Hamiltonian (38), assuming a BMB crystal. Separation will be driven by lowering the external potential to zero, similar to the separation in Sec. III. In contrast to what is described in Sec. III, the curvature of the trapping potential proportional to $k_D(t)$ is increased starting at $t = 0$ to squeeze and couple the modes while the ions experience substantial Coulomb interaction. Additionally, this modulation decreases the distance between the ions and effectively "tensions the springs" before separation. The curvature is ramped up and down quickly over $\tau_1 = 0.85\,\mu\text{s}$ to near zero confinement such that the ions fly apart driven by their mutual Coulomb repulsion. As the trap is of small but nonzero strength with frequency $\omega_{\text{op}} = \omega_0/30$, the B ions reach a distance of 50 μm from their starting equilibrium position at $t_{\text{catch}} \sim 1.4\,\mu\text{s}$, far enough apart to create individual potential minima close to the position of all three ions. The individual potential curvatures are increased and further modulated, and the positions of the B minima move further apart to near ±80 μm ion distance while also providing a decelerating force that is proportional to the velocity of the B ions analogous to (43) to bring them to rest over $\tau_2 = 1.4\,\mu\text{s}$. The modulation of the curvature transforms the final modes back to near their ground states at $t = t_f = t_{\text{catch}} + \tau_2 \approx 2.8\,\mu\text{s}$ after which the external potential is held constant. All in all, the time dependence of the well frequency that the B and M ions experience is

$$\omega_{B,M}(t) = \begin{cases} \omega_0, & t < 0, \\ \omega_{\text{down}}(t), & 0 \leqslant t < \tau_1, \\ \omega_{\text{op}} = \omega_0/30, & \tau_1 \leqslant t < t_{\text{catch}}, \\ \omega_{\text{catchB,M}}(t), & t_{\text{catch}} \leqslant t < t_{\text{catch}} + \tau_2, \\ \omega_0, & t_{\text{catch}} + \tau_2 \leqslant t = t_f, \end{cases} \tag{73}$$

where $\omega_B^2(t) = k_B(t)/m_B$ and $\frac{m_B}{m_M}\omega_M^2(t) = k_M(t)/m_M$. The scaling of $\omega_M^2(t)$ by the ratio of masses is so that both $\omega_M(0) = \omega_0$ and $k_M(0) = k_B(0) \equiv k_0$ hold at $t = 0$. We represent the time-dependent parts of the profile, $\omega_m(t)$ ($m \in \{\text{down}, \text{catchB}, \text{catchM}\}$), by a truncated Fourier series, which can provide a description of arbitrary time dependence with relatively few parameters (compared to other approaches such as splines),

$$\frac{\omega_m(t)}{\omega_0} = a_0 + \sum_{\ell=1}^{4}\left(a_\ell \cos\frac{\pi\,\ell t}{2\tau_m} + b_\ell \sin\frac{\pi\,\ell t}{2\tau_m}\right), \tag{74}$$

with a_ℓ and b_ℓ being the Fourier components, τ_m the amount of time the potential is modulated for, and ω_0 the initial well frequency. For the first modulation, ω_{down}, several of the Fourier components are constrained by the following boundary conditions:

$$\omega_{\text{down}}(0) = \omega_0, \quad \omega'_{\text{down}}(0) = 0, \tag{75}$$

$$\omega_{\text{down}}(\tau_1) = \omega_{\text{op}}, \quad \omega'_{\text{down}}(\tau_1) = 0, \tag{76}$$

The minimum of the catching potential for the B moving in the positive direction moves along $c_c(t) = c_B(t) - \eta\dot{c}_B(t)$, where $c_b(t)$ is the classical position of this B. For the B ion moving in the negative direction, the catching potential position is moving equal and opposite. Hence, the catching potentials implement a force to slow the ions that is proportional to their classical velocity. The time dependence of the catching potential frequencies will be described by another truncated Fourier series (74) with altered boundary conditions, namely initial frequency ω_{op} and final frequency ω_0.

If the unconstrained Fourier components of both the initial well modulation and catching potentials are chosen correctly, modes will be left in their approximate ground states at t_f. Figure 3 illustrates one example of this procedure. The Fourier components are

$$\begin{aligned} (a_0, a_1, a_2, a_3, a_4)_{\text{down}} &= (2.217, 0.3, -0.517, -0.5, -0.5), \\ (b_1, b_2, b_3, b_4)_{\text{down}} &= (-2.2, 0.1, 0.0, 0.5), \\ (a_0, a_1, a_2, a_3, a_4)_{\text{catchB}} &= (24.2, 172.7, -206.5, -0.5, 11.1), \\ (b_1, b_2, b_3, b_4)_{\text{catchB}} &= (-202.3, -0.1, 9.5, 43.5), \end{aligned}$$

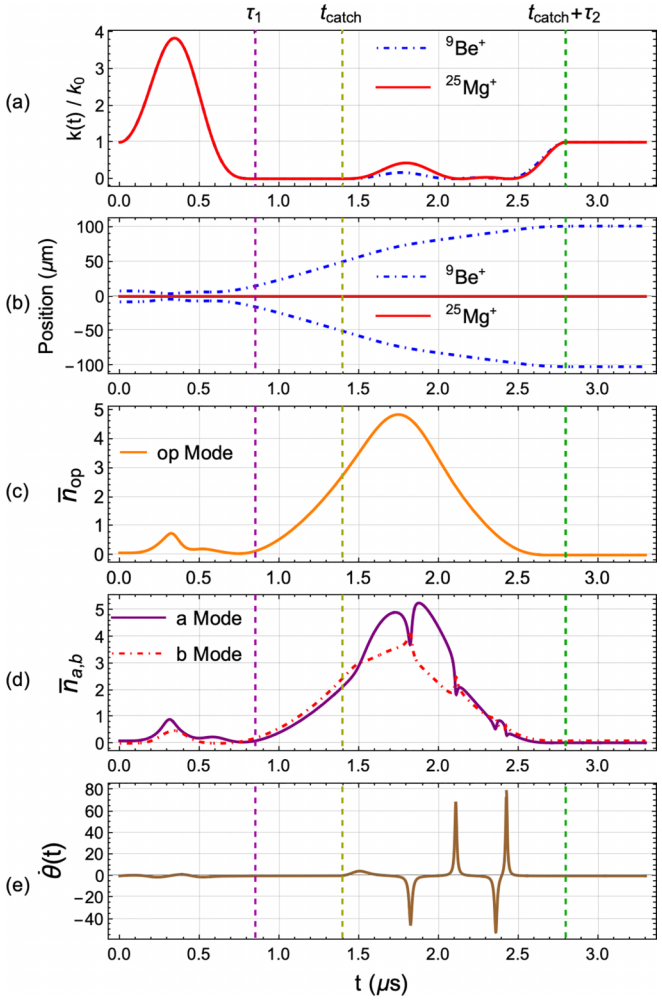

FIG. 3. Spring constants, classical ion positions, numerical solutions for all three modes' average occupation number, and time-derivative of the mixing angle θ. (a) Axial mode well curvature $k(t)/k_0$ for a single ion over time. Red (solid curve) corresponds to the curvature that a trapped single $^{25}Mg^+$ ion experiences, and blue (dot dashed) corresponds to the curvature that the $^9Be^+$ ions experience. (b) Classical positions of the M ion (red, solid) and the two B ions (blue, dot-dashed). Initially the ions are pushed together and then rapidly move apart, while the trapping potential is modulated up and then ramps down to reach a minimal value [leftmost dashed vertical line in (a)–(e)]. After the B ions reach $\approx \pm 50\,\mu$m distance from the M position, individual potentials are turned on that modulate the curvature around the M and the B ions while the B ions are simultaneously decelerated (center dashed line). When all ions come to rest, their occupation numbers are near zero and the potentials are no longer changing (rightmost dashed line). (c) Occupation number of the out-of-phase mode during the time evolution. (d) Occupation numbers of the a and b modes during time evolution. (e) Plot of $\dot{\theta}(t)$ as defined in (38) and (36). The mode interchanging in (d) is caused by the cusplike behavior in $\dot{\theta}$.

$$(a_0, a_1, a_2, a_3, a_4)_{\text{catchM}} = (27.2, 229.5, -264.5, -0.5, 9.3),$$
$$(b_1, b_2, b_3, b4)_{\text{catchM}} = (-260.5, -0.5, 10.5, 57.5). \quad (77)$$

The parameters for this modulated separation were found using a Nelder-Mead numerical optimization scheme such that the total occupation number ($\bar{n}_{\text{op}}$ and $\bar{n}_a + \bar{n}_b$ separately) was minimized.

A perfect implementation of the waveform described by (77) will give final occupation numbers of $\bar{n}_{\text{op}} \sim 0.006$, $\bar{n}_a \sim 0.034$, and $\bar{n}_b \sim 0.11$. As squeezed states in general can have long tails of occupation in the number basis, we also consider the number-basis populations $P_n = |\langle n|\psi_f\rangle|^2$ for the single out-of-phase-mode case and $P_{n,m} = |\langle n_a m_b|\psi_f\rangle|^2$ in the coupled two-mode (ab) case. We state the first few nonzero probabilities here for completeness:

Mode	P_0	P_1	P_2	P_4	P_6
$\|\psi_{\text{op}}\rangle$	0.997	0	0.002 91	1.28×10^{-5}	6.22×10^{-8}
	$P_{0,0}$	$P_{1,1}$	$P_{0,2}$	$P_{2,0}$	$P_{2,2}$
$\|\psi_{ab}\rangle$	0.937	0.0219	0.0326	0.002 97	0.001 03

Here we see that states with odd total quantum number are not occupied, as would be expected from squeezed states. The squeezing parameters for each of the three modes can readily be determined from a Bloch-Messiah decomposition of the final states, and they are given by $r_{\text{op}} \sim 0.0788$, $r_a \sim 0.0289$, and $r_b \sim 0.365$.

This example shows that modulation during separation is feasible, and GGS separation can be executed on the same timescale that describes the Coulomb expansion of a BMB crystal when the potential frequency is dropped from ω_0 to zero (the B ions need approximately 1.3 µs to reach $\pm 80\,\mu$m distance from the M ion in this case). The most time-consuming portion in our example is catching the ions, and while we have not attempted this, it is likely that the entire separation could be sped up further with clever optimization, for example by increasing η from the value of 0.4 µs used in our example.

A. Occupation number response to error in Fourier components

An important consideration for any transport or separation protocol is its robustness to error in its implementation. Here, we address this by introducing random deviations of the Fourier series coefficients. These deviations are supposed to represent random uncontrolled noise, as opposed to static errors that can be compensated for by better calibration. We will introduce random deviations from the intended value in each component in (77) sampled from a uniform distribution with maximum deviation equal to a fraction of the largest Fourier components in each waveform. Results are presented for maximum fractional deviations of 10^{-5} and 5×10^{-5} of the largest Fourier components. Monte Carlo sampling is done from these distributions to produce average final-state populations to characterize the robustness to error.

Recall that during the catching period of this algorithm, the catching potential minima followed the Be^+ ions through (43). However, in a realistic scenario, this trajectory would be precomputed based on an ideal implementation of the Fourier components in (77), which are now disturbed by random error. This random error causes our catching potentials to imper-

TABLE I. Table of Monte Carlo computed average occupations of the out-of-phase mode when the maximum error is 10^{-5} or 5×10^{-5} of the largest Fourier components.

Error	P_0	P_1	P_2	P_3
10^{-5}	0.97	0.025	0.003	0.0002
5×10^{-5}	0.63	0.12	0.056	0.033

fectly slow down the ions, which will in turn oscillate in the final well. The final state can be computed by performing a coherent displacement back into the laboratory frame through a displacement operator,

$$D_f = \exp\left\{\frac{i}{\hbar}[m_B[\dot{c}_{B1}(t_f) - \dot{w}_{B1}(t_f)]x_{B1} + m_B[\dot{c}_{B2}(t_f) - \dot{w}_{B2}(t_f)]x_{B2} - [c_{B1}(t_f) - w_{B1}(t_f)]p_{B1} - [c_{B2}(t_f) - w_{B2}(t_f)]p_{B2}]\right\}, \tag{78}$$

where x_{Bi} are the *original* unscaled operators with units of meters. For simplicity, we do not allow for any asymmetry between the two catching potentials during the slowdown period for the two Be^+ ions, i.e., $c_{B1} = -c_{B2}$. This has the effect of canceling any classical motion effects at the end of transport on the M ion's classical position as well as the a and b modes, which are essentially COM modes, while still providing a realistic assessment of the final state of the out-of-phase mode with noisy potentials. Finally, if the classical trajectory is measured in units of meters and seconds, the displacements of the scaled out-of-phase-mode operators (units of $\sqrt{\text{kg}}$ m and $\sqrt{\text{kg}}$ m/s) are given by

$$D_f^\dagger x_{\text{op}} D_f = x_{\text{op}} + \sqrt{2m_B}[c_{B1}(t_f) - w_{B1}(t_f)], \tag{79}$$

$$D_f^\dagger p_{\text{op}} D_f = p_{\text{op}} + \frac{2}{\sqrt{m_B}} m_B[\dot{c}_{B1}(t_f) - \dot{w}_{B1}(t_f)]. \tag{80}$$

Table I shows the average final transition probability of the out-of-phase mode, while Table II shows the average final transition probabilities of the a and b modes when the error is 1×10^{-5} and 5×10^{-5} of the largest Fourier components. Notably, there is non-negligible occupation in the $n = 1$ state of the out-of-phase mode, which implies that classical motion cannot be neglected even for such a small amount of noise in the waveforms. If the final classical motion were to be neglected, the final occupations of the out-of-phase mode would be more akin to the a and b modes where the only residual occupation is due to imperfect squeezing and mode-mixing. The second row in Table I makes this even more apparent when the error is allowed to increase to 5×10^{-5} and we see non-negligible occupation of the $n = 3$ state. Here we again note that no asymmetry has been introduced into the B ion catching potentials, which would disturb the classical motion of the M ion. This has been done for simplicity, so any real implementation of this protocol must take asymmetric perturbations into account as states like $P_{0,1}$ and $P_{1,0}$ will have nonzero and non-negligible occupation. Furthermore, allowing for asymmetry will bring in nonzero contributions from the cubic correction to the Coulomb potential—these corrections will remain small, but they should be properly considered when implementing the protocol in a realistic scenario. We also note that the same precision in realizing the external potentials is required in implementations with precompensation and simple ramps, such as the one discussed in Sec. III and Ref. [25].

TABLE II. Table of Monte Carlo computed average transition probabilities of the final state for the a and b modes when the error is 10^{-5} of the largest Fourier components. The equivalent table produced when the error is taken to be 5×10^{-5} is essentially indistinguishable from this.

P_a \ P_b	0	1	2	3	4
0	0.94	0	0.032	0	0.0017
1	0	0.022	0	0.0023	0
2	0.0028	0	0.0010	0	0.000 15
3	0	0.000 19	0	0.000 060	0
4	0.000 013	0	0.000 013	0	≈0

This analysis highlights the exquisite control over the Fourier components of the waveform necessary to reliably achieve fast GGS. Slower implementations will improve the robustness, with one limit represented by the essentially adiabatic separation methods that have already been demonstrated. Initial experimental implementations will likely be only slightly faster than adiabatic, and durations will drop as control improves. Small deviations from the ground state can be removed by recooling the DHD crystal on the H ion [53], but recooling must be rapid so as not to defeat the purpose of fast separation, and therefore the modes should have as low as possible occupations after separation.

V. CONCLUSIONS

Rapid separation of a DHD three-ion crystal leads to squeezing and mode-mixing that needs to be carefully managed to end in the quantum-mechanical ground states of all three axial normal modes of the separated ions. To achieve GGS, the effects of separation can either be precompensated by suitable squeezing and mode-mixing operations before separation, or more expediently be mitigated by precisely controlled modulation of the potential during separation. Importantly, we find that there is not a significant time penalty for the latter method when compared to Coulomb expansion after the external trapping potential is instantaneously set to zero. An example implementation uses an efficient Fourier representation of the trapping potential and ideally terminates with all three axial modes close to the ground state. The time dependence of the external potential is smooth, but it requires very precise control that will take effort to implement with realistic driving electronics. Uncontrolled stray potential fluctuations will also need to be carefully minimized. Utilizing the Coulomb repulsion to drive the ions apart rather than narrow separation electrodes that create a "wedge" between ions [54] may help with reducing the complexity and electrode count of traps that are suitable for GGS separation. Separating D ions out of a DHD crystal trapped in a single well allows for the D ions to travel through a larger trap array on their own

so they can be paired with other D ions in subsequent gate operations, while the H ions stay in place. This approach could mitigate issues from transporting groups of ions of different mass through junctions in a large ion trap array [55], and it simplifies transport in general, since all transport primitives besides separation only need to be implemented for the D species. In this context, it is worth noting that recombination of two D ions that approach a stationary H from the opposite directions is the time reversal of DHD separation. Since the equations of motion are invariant under time reversal, ground-state-to-ground-state recombination can be accomplished by running the separation protocol backwards in time. Performing imperfect separation and recombination multiple times will lead to error accumulation from imprecision in the electrode control, higher order than quadratic terms in the potential energy, and fluctuating stray potentials, but small amounts of excess energy can be removed by cooling the H ion when the DHD crystal is confined in a single external well [53]. Further refinement of GGS can reduce the duration of subsequent cooling to a minimum.

Although we do not explicitly show how the procedure in Sec. III D generalizes to crystals with more than three ions, we describe its general implementation and how the effects of separation can be decomposed into single mode squeezing and multiport interferometers. In general, external potential modulations can accomplish diabatic squeezing and mode-mixing operations not just for ground states, but they could be used for implementing complex Gaussian operations on any initial motional state of groups of ions, with the potential for further generalization to all $3N$ motional modes of N ions. This could be of interest in realizing error correction codes and quantum logical operations on bosonic qubits realized in the motion of ion crystals [56,57] and for realizing entangled states of ion internal degrees of freedom generated by coupling them to nonclassical states of the motion with Jaynes-Cummings-type interactions [58].

ACKNOWLEDGMENTS

The authors would like to thank T. Sutherland for useful discussions. The work of D.L. and D.H.S. was supported by the NIST Quantum Information Program. The work of T.H.G. and S.B.L. was performed under the auspices of the U.S. Department of Energy by Lawrence Livermore National Laboratory under Contract No. DE-AC52-07NA27344.

[1] D. J. Wineland, C. Monroe, W. M. Itano, D. Leibfried, B. E. King, and D. M. Meekhof, Experimental issues in coherent quantum-state manipulation of trapped atomic ions, J. Res. Natl. Inst. Stand. Technol. **103**, 259 (1998).

[2] D. Kielpinski, C. Monroe, and D. Wineland, Architecture for a large-scale ion-trap quantum computer, Nature (London) **417**, 709 (2002).

[3] J. M. Pino *et al.*, Demonstration of the trapped-ion quantum CCD computer architecture, Nature (London) **592**, 209 (2021).

[4] S. A. Moses *et al.*, A race-track trapped-ion quantum processor, Phys. Rev. X **13**, 041052 (2023).

[5] R. Bowler, J. Gaebler, Y. Lin, T. R. Tan, D. Hanneke, J. D. Jost, J. P. Home, D. Leibfried, and D. J. Wineland, Coherent diabatic ion transport and separation in a multizone trap array, Phys. Rev. Lett. **109**, 080502 (2012).

[6] A. Walther, F. Ziesel, T. Ruster, S. T. Dawkins, K. Ott, M. Hettrich, K. Singer, F. Schmidt-Kaler, and U. Poschinger, Controlling fast transport of cold trapped ions, Phys. Rev. Lett. **109**, 080501 (2012).

[7] J. D. Sterk, H. Coakley, J. Goldberg, V. Hietala, J. Lechtenberg, H. McGuinness, D. McMurtrey, L. P. Parazzoli, J. Van Der Wall, and D. Stick, Closed-loop optimization of fast trapped-ion shuttling with sub-quanta excitation, npj Quantum Inf. **8**, 68 (2022).

[8] C. R. Clark *et al.*, Characterization of fast ion transport via position-dependent optical deshelving, Phys. Rev. A **107**, 043119 (2023).

[9] H. Kaufmann, T. Ruster, C. T. Schmiegelow, M. A. Luda, V. Kaushal, J. Schulz, D. von Lindenfels, F. Schmidt-Kaler, and U. G. Poschinger, Fast ion swapping for quantum-information processing, Phys. Rev. A **95**, 052319 (2017).

[10] M. Rowe *et al.*, Transport of quantum states and sepration of ions in a dual rf ion trap, Quant. Inf. Comp. **2**, 257 (2002).

[11] M. D. Barrett *et al.*, Deterministic quantum teleportation of atomic qubits, Nature (London) **429**, 737 (2004).

[12] J. P. Home, D. Hanneke, J. D. Jost, J. M. Amini, D. Leibfried, and D. J. Wineland, Complete methods set for scalable ion trap quantum information processing, Science **325**, 1227 (2009).

[13] R. B. Blakestad, C. Ospelkaus, A. P. Van Devender, J. M. Amini, J. Britton, D. Leibfried, and D. J. Wineland, High-fidelity transport of trapped-ion qubits through an **X**-junction trap array, Phys. Rev. Lett. **102**, 153002 (2009).

[14] Y. Wan *et al.*, Quantum gate teleportation between separated qubits in a trapped-ion processor, Science **364**, 875 (2019).

[15] F. Lancellotti, S. Welte, M. Simoni, C. Mordini, T. Behrle, B. de Neeve, M. Marinelli, V. Negnevitsky, and J. P. Home, Low-excitation transport and separation of high-mass-ratio mixed-species ion chains, Phys. Rev. Res. **6**, L032059 (2024).

[16] E. Torrontegui, S. Ibáñez, X. Chen, A. Ruschhaupt, D. Guéry-Odelin, and J. G. Muga, Fast atomic transport without vibrational heating, Phys. Rev. A **83**, 013415 (2011).

[17] H.-K. Lau and D. F. V. James, Decoherence and dephasing errors caused by the dc stark effect in rapid ion transport, Phys. Rev. A **83**, 062330 (2011).

[18] H. Kaufmann, T. Ruster, C. T. Schmiegelow, F. Schmidt-Kaler, and U. G. Poschinger, Dynamics and control of fast ion crystal splitting in segmented Paul traps, New J. Phys. **16**, 073012 (2014).

[19] M. Palmero, R. Bowler, J. P. Gaebler, D. Leibfried, and J. G. Muga, Fast transport of mixed-species ion chains within a Paul trap, Phys. Rev. A **90**, 053408 (2014).

[20] M. Palmero, S. Martínez-Garaot, U. G. Poschinger, A. Ruschhaupt, and J. G. Muga, Fast separation of two trapped ions, New J. Phys. **17**, 093031 (2015).

[21] T. Ruster, C. Warschburger, H. Kaufmann, C. T. Schmiegelow, A. Walther, M. Hettrich, A. Pfister, V. Kaushal, F. Schmidt-Kaler, and U. G. Poschinger, Experimental realization of fast ion separation in segmented Paul traps, Phys. Rev. A **90**, 033410 (2014).

[22] H.-K. Lau, Diabatic ion cooling by phonon swapping during controlled collision, Phys. Rev. A **90**, 063401 (2014).
[23] I. Lizuain, M. Palmero, and J. G. Muga, Dynamical normal modes for time-dependent Hamiltonians in two dimensions, Phys. Rev. A **95**, 022130 (2017).
[24] S. Simsek and F. Mintert, Quantum invariant-based control of interacting trapped ions, arXiv:2112.13905.
[25] R. T. Sutherland, S. C. Burd, D. H. Slichter, S. B. Libby, and D. Leibfried, Motional Squeezing for Trapped Ion Transport and Separation, Phys. Rev. Lett. **127**, 083201 (2021).
[26] P. Ehrenfest, Bemerkung über die angenäherte Gültigkeit der klassischen Mechanik innerhalb der Quantenmechanik, Z. Phys. **45**, 455 (1927).
[27] E. J. Heller, Time–dependent approach to semiclassical dynamics, J. Chem. Phys. **62**, 1544 (1975).
[28] D. Huber and E. J. Heller, Generalized Gaussian wave packet dynamics, J. Chem. Phys. **87**, 5302 (1987).
[29] C. Bloch and A. Messiah, The canonical form of an antisymmetric tensor and its application to the theory of superconductivity, Nucl. Phys. **39**, 95 (1962).
[30] R. Simon, E. C. G. Sudarshan, and N. Mukunda, Gaussian-Wigner distributions in quantum mechanics and optics, Phys. Rev. A **36**, 3868 (1987).
[31] A. M. Perelomov, Coherent states for arbitrary lie group, Commun. Math. Phys. **26**, 222 (1972).
[32] K. Wodkiewicz and J. H. Eberly, Coherent states, squeezed fluctuations, and the $SU(2)$ am $SU(1,1)$ groups in quantum-optics applications, J. Opt. Soc. Am. B **2**, 458 (1985).
[33] C. C. Gerry, Dynamics of SU(1,1) coherent states, Phys. Rev. A **31**, 2721 (1985).
[34] B. Yurke, S. L. McCall, and J. R. Klauder, SU(2) and SU(1,1) interferometers, Phys. Rev. A **33**, 4033 (1986).
[35] J.-W. Wu, C.-W. Li, R.-B. Wu, T.-J. Tarn, and J. Zhang, Quantum control by decomposition of $SU(1, 1)$, J. Phys. A **39**, 13531 (2006).
[36] B. C. Hall, An elementary introduction to groups and representations, arXiv:math-ph/0005032.
[37] C. Weedbrook, S. Pirandola, R. García-Patrón, N. J. Cerf, T. C. Ralph, J. H. Shapiro, and S. Lloyd, Gaussian quantum information, Rev. Mod. Phys. **84**, 621 (2012).
[38] R. Simon, E. Sudarshan, and N. Mukunda, Gaussian Wigner distributions: A complete characterization, Phys. Lett. A **124**, 223 (1987).
[39] Arvind, B. Dutta, N. Mukunda, and R. Simon, The real symplectic groups in quantum mechanics and optics, Pramana **45**, 471 (1995).
[40] D. J. Heinzen and D. J. Wineland, Quantum-limited cooling and detection of radio-frequency oscillations by laser-cooled ions, Phys. Rev. A **42**, 2977 (1990).
[41] D. M. Meekhof, C. Monroe, B. E. King, W. M. Itano, and D. J. Wineland, Generation of nonclassical motional states of a trapped atom, Phys. Rev. Lett. **76**, 1796 (1996).
[42] H.-Y. Lo, D. Kienzler, L. de Clercq, M. Marinelli, V. Negnevitsky, B. C. Keitch, and J. P. Home, Spin–motion entanglement and state diagnosis with squeezed oscillator wavepackets, Nature (London) **521**, 336 (2015).
[43] S. C. Burd, R. Srinivas, J. J. Bollinger, A. C. Wilson, D. J. Wineland, D. Leibfried, D. H. Slichter, and D. T. C. Allcock, Quantum amplification of mechanical oscillator motion, Science **364**, 1163 (2019).
[44] R. Simon, N. Mukunda, and B. Dutta, Quantum-noise matrix for multimode systems: U(n) invariance, squeezing, and normal forms, Phys. Rev. A **49**, 1567 (1994).
[45] L. F. Hackl, Aspects of Gaussian states entanglement, squeezing and complexity, Ph.D. thesis, Penn State University, 2018.
[46] J. B. Brask, Gaussian states and operations – a quick reference, arXiv:2102.05748.
[47] G. Schrade, P. J. Bardroff, R. J. Glauber, C. Leichtle, V. Yakovlev, and W. P. Schleich, Endoscopy in the Paul trap: The influence of the micromotion, Appl. Phys. B **64**, 181 (1997).
[48] S. L. Braunstein, Squeezing as an irreducible resource, Phys. Rev. A **71**, 055801 (2005).
[49] M. Reck, A. Zeilinger, H. J. Bernstein, and P. Bertani, Experimental realization of any discrete unitary operator, Phys. Rev. Lett. **73**, 58 (1994).
[50] W. R. Clements, P. C. Humphreys, B. J. Metcalf, W. S. Kolthammer, and I. A. Walmsley, Optimal design for universal multiport interferometers, Optica **3**, 1460 (2016).
[51] G. Cariolaro and G. Pierobon, Reexamination of Bloch-Messiah reduction, Phys. Rev. A **93**, 062115 (2016).
[52] P.-Y. Hou *et al.*, Coherent coupling and non-destructive measurement of trapped-ion mechanical oscillators, Nat. Phys. (2024), doi:10.1038/s41567-024-02585-y.
[53] P.-Y. Hou, J. J. Wu, S. D. Erickson, G. Zarantonello, A. D. Brandt, D. C. Cole, A. C. Wilson, D. H. Slichter, and D. Leibfried, Indirect cooling of weakly coupled trapped-ion mechanical oscillators, Phys. Rev. X **14**, 021003 (2024).
[54] J. P. Home and A. M. Steane, Electrode configurations for fast separation of trapped ions, Quantum Inf. Comput. **6**, 289 (2006).
[55] W. C. Burton, B. Estey, I. M. Hoffman, A. R. Perry, C. Volin, and G. Price, Transport of multispecies ion crystals through a junction in a radio-frequency Paul trap, Phys. Rev. Lett. **130**, 173202 (2023).
[56] D. Gottesman, A. Kitaev, and J. Preskill, Encoding a qubit in an oscillator, Phys. Rev. A **64**, 012310 (2001).
[57] C. Flühmann, T. L. Nguyen, M. Marinelli, V. Negnevitsky, K. Mehta, and J. P. Home, Encoding a qubit in a trapped-ion mechanical oscillator, Nature (London) **566**, 513 (2019).
[58] D. J. Wineland, J. J. Bollinger, W. M. Itano, and D. J. Heinzen, Squeezed atomic states and projection noise in spectroscopy, Phys. Rev. A **50**, 67 (1994).